Parameterization of the collision-coalescence process using series of basis functions: *COLNETv1.0.0* model development using a machine learning approach

Camilo Fernando Rodríguez-Genó[1], Léster Alfonso[2]

[1]Atmospheric Sciences Centre, National Autonomous University of Mexico, Mexico City, 04510, Mexico
[2]Autonomous University of Mexico City, Mexico City, 09790, Mexico

Correspondence to: Camilo Fernando Rodríguez Genó (camilo.rodriguez@atmosfera.unam.mx)

Abstract. A parameterization for the collision-coalescence process is presented, based on the methodology of basis functions. The whole drop spectrum is depicted as a linear combination of two lognormal distribution functions, leaving no parameters fixed. This basis-function parameterization avoids the classification of drops in artificial categories such as cloud water (cloud droplets) or rain water (raindrops). The total moment tendencies are predicted using a machine learning approach, in which one deep neural network was trained for each of the total moment orders involved. The neural networks were trained using randomly generated data , over a wide range of parameters employed by the parameterization. An analysis of the predicted total moment errors was performed, aimed to establish the accuracy of the parameterization at reproducing the integrated distribution moments representative of physical variables. The applied machine learning approach shows a good accuracy level when compared to the output of an explicit collision-coalescence model.

Keywords: cloud microphysics; collision-coalescence; lognormal distribution; microphysics parameterization; numerical modelling; machine learning; neural networks.

1 Introduction

Drop populations are represented using drop size distributions (DSD). The first attempt at characterizing drop spectra was made by Marshall and Palmer (1948), who employed exponential distributions based on drop diameter to describe the DSDs (Marshall and Palmer, 1948). More recently, the use of a three-parameter gamma distribution has shown a good agreement with observations (Ulbrich, 1983). However, lognormal distributions have shown a better squared-error fit to measurements of rain DSDs than gamma or exponential distributions (Feingold and Levin, 1986; Pruppacher and Klett, 2010). The analysis of several important characteristics of the Brownian coagulation process showed that the lognormal distribution adequately represents the particle distributions (Lee et al., 1984, 1997). In addition, some authors have employed this type of distribution function, lognormal, to parameterize cloud processes with promising results (Clark, 1976; Feingold et al., 1998; Huang, 2014).

There are two main approaches to modelling cloud processes: the explicit approach (bin microphysics) and the bulk approach (bulk microphysics). Bin microphysics is based on the discretization of a DSD into sections (bins), and calculates the evolution of the DSD due to the influence of different processes that could be dynamical and/or microphysical (Berry, 1967; Berry and Reinhardt, 1974; Bott, 1998a; Khain et al., 2004, 2010). The core of this method is the solution of the Kinetic Coagulation Equation (KCE) (von Smoluchowski, 1916a, 1916b) for the collision-coalescence of liquid drops, (also known as Stochastic Coalescence Equation or Kinetic Collection Equation within the cloud physics community), in a previously designed grid, which could be over mass or radius. Thus, previous knowledge of the characteristics or parameters of the distributions is not necessary. This way of solving the KCE is very accurate, but its operational utility is compromised because it is computationally very expensive, due to the need to calculate a large number of equations, ranging from several dozens to hundreds, at each grid point and time step. Besides, as the KCE has no analytical solution, it has to be solved via numerical schemes, which are very diffusive by nature. While diffusive schemes could be appropriate for certain microphysical processes such as sedimentation (Khain et al., 2015), it is a disadvantage that has to be dealt with. However, the numerical solutions of the KCE have evolved in such a way that today we can find models that are specifically design to limit the diffusiveness of these numerical methods (Bott, 1998a). In the case of bulk microphysics, the KCE is parameterized and the evolution of a chosen set of statistical moments related to physical variables is calculated, instead of the evolution of the DSD itself. A pioneer approach to this kind of parameterizations can be found in Kessler (1969), where a simple but relatively accurate representation of the autoconversion process is introduced. One or two-moment parameterizations are common (Cohard and Pinty, 2000; Lim and Hong, 2010; Milbrandt and McTaggart-Cowan, 2010; Morrison et al., 2009; Thompson et al., 2008). However, recently it has been extended to three-moment parameterizations (Huang, 2014; Milbrandt and Yau, 2005). This type of parameterization is computationally efficient, which makes it popular within the operational weather forecasting community. The main disadvantage of this approach is that the equations for solving the rates of the p-th moment include moments of a higher order, so the system of equations employed to calculate the evolution of the moments is not closed (Seifert and Beheng, 2001). This could be avoided by using predefined parameters for the distributions that describe the DSD, which normally take the form of exponential (Marshall and Palmer, 1948), gamma (Milbrandt and McTaggart-Cowan, 2010; Milbrandt and Yau, 2005) or lognormal distributions (Huang, 2014). Besides, artificial categories are often used to separate hydrometeors (cloud and rain water), depending on drop radius, values between 20 μm and 41 μm are very popular thresholds (Cohard and Pinty, 2000; Khairoutdinov and Kogan, 2000), with the moments for each category being calculated by means of partial integration of the KCE.

An additional approach to modelling microphysical processes is the particle-based one, which is based on the application of a stochastic model such as the Monte Carlo method to the coagulation (coalescence) of drop particles inside a cloud. This method has been approached from a number of perspectives. For example Alfonso et al. (2008) analysed the possible ways of solving the KCE by using a Monte Carlo algorithm and several collision kernels, with good correspondence between the analytical and numerical approaches for all the kernels, by estimating the KCE following Gillespie’s Monte Carlo algorithm (Gillespie, 1972) and several analytical solutions. Also, the possible implications of this approach for cloud physics are discussed. Other variants of this approach are analysed in Alfonso et al. (2011), and it has also been used to simulate the subprocesses of autoconversion and accretion applying a Monte Carlo-based algorithm within the framework of Lagrangian cloud models (Noh et al., 2018). This approach is accurate, and represents well the stochastic nature of the collision-coalescence of drops, but it is very expensive computationally.

An alternative to these main approaches is a hybrid approach to parameterize the cloud microphysical processes. This approach simulates the explicit approach in the way that it describes the shape of the DSD through a linear combination of basis functions (Clark, 1976; Clark and Hall, 1983), and it could be considered a middle point between bulk and bin microphysics. This is done by having time-varying distribution parameters, instead of fixed ones, as is common in conventional bulk approaches. A system of prognostic equations is solved to obtain the parameters' tendencies related to the statistical distribution functions based on the evolution of their total moments (the combination of the statistical moments with same order of all distribution functions involved), describing their tendencies due to condensation and collision-coalescence. Since the integration process covers the entire size spectrum, the artificial separation of the droplet spectrum is avoided, making the terms cloud droplet and rain drop meaningless (they are just drops), and it is possible to solve a fully closed system of equations without the need to keep any parameter of the distribution constant. However, this integration can be made only once for all parameters at each time step. Another advantage of this approach is its independence from a specific collision kernel type, as is common in the bulk approach; in order to obtain analytical expressions from the integrals of the KCE, a polynomial type kernel such as the one derived by Long(1974) is frequently used. Having said that, a limitation of this approach is that the total moment tendencies have to be solved at each time step for the needed parameters. An alternative solution for this shortcoming is previously calculating the moment's rates by including a sufficiently wide range of parameters, and store the results in lookup tables that should be consulted several times at every time step.

Machine Learning (ML) is the study of computer algorithms that improve automatically through experience and by the use of data (training) (Mitchell, 1997). ML algorithms build a model based on sample data in order to make predictions or decisions without being explicitly programmed to do so (Koza et al., 1996). They are used in a wide variety of applications, such as in medicine, email filtering, and computer vision, where it is difficult or unfeasible to develop conventional algorithms to perform the needed tasks. In particular, neural networks (NN) are especially well suited for solving non-linear fitting problems and for establishing relationships within complex data such as the outputs of the KCE. In the field of atmospheric sciences, the use of DNNs has been extended to the parameterization of subgrid processes in climate models (Brenowitz and Bretherton, 2018; Rasp et al., 2018), while in cloud microphysics, the autoconversion process was parameterized using DNNs with a superior level of accuracy when compared with equivalent bulk models (Alfonso and Zamora, 2021; Sobhani et al., 2018). Also, a partial parameterization of collision-coalescence was tested in Seifert and Rasp(2020), which developed a ML parameterization that includes the processes of autoconversion and accretion, describing the droplet spectra as a gamma distribution, and establishing a comparative study that exposed the advantages and disadvantages of the use of ML techniques on cloud microphysics.

In order to eliminate the need to solve the rate equations for the total moments of the KCE at every time step (Thompson, 1968), or resort to the use of lookup tables, we propose to predict the total moment tendencies using a ML approach within this parameterization. With this approach, the use of one trained Deep Neural Network (DNN) for each calculated total moment tendency will accelerate the calculations without sacrificing precision. Thus, the objective of this study is to apply DNN to the parameterized formulation of the collision-coalescence process developed by Clark(1976) in order to replicate the rate equations for the total moments, eliminating the need of memory expensive lookup tables or processing-time expensive numerical solution of integrals.

The research article is structured as follows: In section 2, the parameterization framework is described, as well as the reference model used for comparison purposes; In section 3, the procedures of DNN methodology are explained and the network architecture is introduced, the training data set is generated, and the DNN is trained and validated; In section 4, the experiment design is explained; In section 5, the results are discussed, an assessment of the results is made by contrasting them with the reference solution, and the predicted total moment errors are analyzed; and in section 6 several conclusions are drawn.

2 Description of the collision-coalescence parameterization

2.1 Formulation of the total moment tendencies

Under the framework of the parameterization developed in this study, any given drop spectrum can be approximated by a series of basis functions. Therefore, the distribution that characterizes the evolution of the spectrum is given by a linear combination of probability density functions as shown below:

$$f\langle r\rangle = \sum_{i=1}^{I} f_i\langle r\rangle \qquad (1)$$

where $f_i\langle r\rangle$ are the individual members of the set of distributions considered, I stands for the number of distribution functions that make up the set, and r refers to the radius of drops. In the case at hand, a set of two statistical distributions is employed. At each time step, the rates of the parameters of each distribution will be calculated. It should be noted that, in any set of distributions considered, all the members have the same type of distribution. For the proposed parameterization, as described in Clark(1976), a distribution of log-normal type is used, as follows

$$f\langle r\rangle = \frac{N}{\sqrt{2\pi}\sigma r} e^{[-(ln\, r-\mu)^2/(2\sigma^2)]} \qquad (2)$$

Where μ and σ^2 stand for the mean and variance of $\ln r$ respectively, while N represents the number concentration of drops. Considering that moment of order p ($\overline{R^p}$) of any distribution can be defined as (Straka, 2009)

$$N\overline{R^p} = \int_0^\infty r^p f(r) dr \qquad (3)$$

the following analytical solution of eq. (3) can be found for the moments of the lognormal distribution

$$\overline{R^p} = e^{p\mu + \frac{1}{2}p^2\sigma^2} \qquad (4)$$

Combining eqs. (1), (3) and (4), the *p*-th total moment of a linear combination of lognormal distributions could be expressed as (Clark and Hall, 1983)

$$N\overline{R^p} = \sum_{i=1}^{I} N_i \overline{R_i^p} = \sum_{i=1}^{I} N_i e^{p\mu_i + \frac{1}{2}p^2\sigma_i^2} \qquad (5)$$

Where the index *i* indicates each of the individual members of the set (*I=2*). Deriving eq. (5) with respect to time, we obtain the tendencies of the total moments of a series of log-normal distributions

$$\frac{\partial N\overline{R^p}}{\partial t} = \sum_{i=1}^{I} N_i \overline{R_i^p} \left(\frac{\partial \ln N_i}{\partial t} + p \frac{\partial \mu_i}{\partial t} + \frac{p^2}{2} \frac{\partial {\sigma_i}^2}{\partial t} \right) \qquad (6)$$

Equation (6) can be expressed as a system of equations

$$\boldsymbol{AX} = \boldsymbol{F} \qquad (7)$$

where **X** is a vector representing the tendencies of the distribution parameters

$$X^T = \left[\frac{\partial \ln N_1}{\partial t}, \frac{\partial \ln N_2}{\partial t}, \ldots, \frac{\partial \ln N_I}{\partial t}, \frac{\partial \mu_1}{\partial t}, \frac{\partial \mu_2}{\partial t}, \ldots, \frac{\partial \mu_I}{\partial t}, \frac{\partial {\sigma^2}_1}{\partial t}, \frac{\partial {\sigma^2}_2}{\partial t}, \ldots, \frac{\partial {\sigma^2}_I}{\partial t} \right] \qquad (8)$$

The coefficient's matrix A is a squared matrix of order ν ($\nu = 3 \times I$) defined as

$$A = \begin{cases} a_{i,j} = N_j \overline{R_j^{\iota-1}} / (N\overline{R^{\iota-1}}) \\ a_{i,j+I} = (i-1) N_j \overline{R_j^{\iota-1}} / (N\overline{R^{\iota-1}}) \\ a_{i,j+2I} = \frac{1}{2}(i-1)^2 N_j \overline{R_j^{\iota-1}} / (N\overline{R^{\iota-1}}) \end{cases} \qquad (9)$$

with $i = 1,2,\ldots,\nu$ and $j = 1,2,\ldots,I$. The components of the independent vector F are the tendencies of the total moments of the distributions:

$$F^T = \left[\frac{\partial \ln N\overline{R^0}}{\partial t}, \frac{\partial \ln N\overline{R^1}}{\partial t}, \ldots, \frac{\partial \ln N\overline{R^{\nu-1}}}{\partial t} \right] \qquad (10)$$

Both **A** and **F** are normalized in order to achieve a better numerical stability in the solution of the system of equations. The evolution of the distribution functions' parameters is calculated by applying a simple forward finite differences scheme (Clark and Hall, 1983)

$$N_i^{k+1} = N_i^k e^{\frac{\partial \ln N_i^k}{\partial t} \Delta t} \qquad (11a)$$

$$\mu_i^{k+1} = \mu_i^k + \frac{\partial \mu_i^k}{\partial t}\Delta t \qquad (11b)$$

$$(\sigma^2)_i^{k+1} = (\sigma^2)_i^k + \frac{\partial (\sigma^2)_i^k}{\partial t}\Delta t \qquad (11c)$$

With *k* being the time index in the finite difference's notation.

2.2 Description of the calculation of the total moment tendencies due to collision-coalescence

The KCE determines the evolution of a DSD due to collision-coalescence. This equation can be expressed in a continuous form as a function of mass as follows (Pruppacher and Klett, 2010)

$$\frac{\partial f}{\partial t} = \int_0^{m/2} f(m-m')f(m')K(m-m'|m')dm' - \int_0^{\infty} f(m)f(m')K(m|m')dm' \qquad (12)$$

where $K(m|m')$ is the collection kernel. Reformulating eq. (12) in the form of Thompson(1968) and in function of radius, we can calculate the total moment tendencies (vector **F** from the previous section) as follows

$$\frac{dN\overline{R^p}}{dt} = \frac{1}{2}\int_0^{\infty}\int_0^{\infty} F^p(r_1,r_2)K(r_1|r_2)f\langle r_1\rangle f\langle r_2\rangle dr_1 dr_2 \qquad (13)$$

where

$$F^p(r_1,r_2) = (r_1^3 + r_2^3)^{p/3} - r_1^p - r_2^p \qquad (14)$$

$$K\langle r_1|r_2\rangle = \pi(r_1+r_2)^2 E(r_1,r_2)|V_T(r_1) - V_T(r_2)| \qquad (15)$$

Equation (15) represents the hydrodynamic kernel and $E(r_1,r_2)$ stands for the collection efficiencies taken from Hall(1980), which is based on a lookup table representing the effectiveness of drop collisions under given environmental conditions. A set of two lognormal distributions (eq. (2)) is used as members of the set in eq. (1). Hence, the prognostic variables under the parameterization formulation will be the corresponding parameters of both distribution functions: N_1, μ_1 , σ_1, N_2, μ_2 and σ_2. At this point in the parameterization the total moment tendencies should be calculated either by solving eq. (13) at each time step for all the moments involved, or by searching in a lookup table calculated a priori. Instead, the following section explains in detail the ML approach proposed and its implementation.

2.3 Description of the reference model

To obtain a reference solution (KCE from now onwards), the explicit model developed by Bott(1998a) was employed. This scheme is conservative with respect to mass and very efficient computationally speaking. It is based on the numerical integration of the KCE which, rewritten in a more convenient way, is expressed as shown below:

$$\frac{dn(x,t)}{dt} = \int_{x_0}^{x_1} n(x_c,t)K(x_c,\ x')n(x',t)dx' - \int_{x_0}^{\infty} n(x,t)K(x,x')n(x',t)dx' \tag{16}$$

where $n(x,t)$ stands for the DSD at time *t* and $K(x_c,\ x')$ represents the collection kernel. In order to simplify the calculations, the mass density function $g(y,t)$ is used (Berry, 1967):

$$g(y,t)dy = xn(x,t)dx \tag{17}$$

$$n(x,t) = \frac{1}{3x^2}g(y,t) \tag{18}$$

where $y = \ln r$ and *r* is the radius of a drop of mass *x*. By substituting (21) in (20) we obtain the KCE for the mass density function (Bott, 1998a)

$$\frac{dg(y,t)}{dt} = \int_{y_0}^{y_1} \frac{x^2}{x_c^2 x'} g(y_c,t)K(y_c,\ y')g(y',t)dy' - \int_{y_0}^{\infty} g(y,t)\frac{K(y,y')}{x'}g(y',t)dy' \tag{19}$$

The first integral of the right-hand side of eq. (19) represents the gain of drops of mass *x* due to collision-coalescence of two smaller droplets, while the second integral portrays the loss of drops of mass *x* being captured by bigger drops (Bott, 1998a). For the numerical solution of eq. (19), a logarithmic equidistant mass grid is used, and is generated as

$$x_{k+1} = \alpha x_k, \qquad k = 1,2,\dots,m \tag{20}$$

where *m* is the total number of grid points. The original code for this explicit model can be found at (Bott, 1998b), and can be used with authorization of the author.

3 Machine Learning architecture and training data set

ML methodology can be classified into three main categories, according to the problem at hand: supervised, unsupervised and reinforced learning. In our case, supervised learning is used. Supervised learning algorithms build a mathematical model of a set of data that contains both the inputs and the desired outputs (Russell and Norvig, 2010). Under this classification, there is previous knowledge of the set of input values $\vec{x}_k$, and their corresponding outputs $\vec{y}_k$, , with $k = 1,2,\dots,n$, where n is the amount of input values. The objective is to obtain a function $f(\vec{x})$, by means of which the new data $\vec{x}_{new}$ simulates reasonably well the output values. The set $\{\vec{x}_k, \vec{y}_k\}$; $k = 1,2,\dots,n$ is called the training data set. To test the performance of $f(\vec{x})$, the input and output data are separated into two different data sets: training and testing. As NN are able to fit any non-linear function (Schmidhuber, 2015), a ML parameterization should approximate reasonably well the solution of the KCE in the form of eq. (13), given enough layers and neurons in the architecture of the network.

3.1 Neural network architecture

Deep Neural Networks are based on artificial neurons. Each neuron receives a set of input data, processes it and passes it to an activation function $\sigma(z)$, which returns the activated output (Fig. 1). The activation value of neuron *i* in layer *l* is denoted by a_i^l and is determined as

$$a_i^l = \sigma\left(z_i^l\right) \qquad (21)$$

$$z_i^l = b_i^l + \sum_{j=!}^{m_l-1} W_{i,j}^l x_i^{l-1} \qquad (22)$$

In eq. (22), b_i^l is the bias, $W_{i,j}^l$ is the ponderation weight, m_{l-1} the number of neurons in layer *l-1*,, $\sigma(z)$ is the activation function, and *z* is the processing intermediate value of the variable. Hence, a NN could be defined as a set of input values ($\vec{x}$), bias values ($\vec{b}$) and weights ($\vec{W}$) integrated in a functional form, i.e. $\vec{y}\left(\vec{x}, \vec{W}, \vec{b}\right)$, and its training procedure consists of minimizing an error function (known as loss function), by optimizing the weights and biases for the available training data. A commonly used loss function is the regression mean squared error (MSE). Hence, we need a minimization algorithm to process the following expression

$$C\left(\vec{W}, \vec{b}\right) = \frac{1}{2n}\sum_k \left\|\vec{y}\left(\vec{x}_k, \vec{W}, \vec{b}\right) - \vec{y}_k\right\|^2 \qquad (23)$$

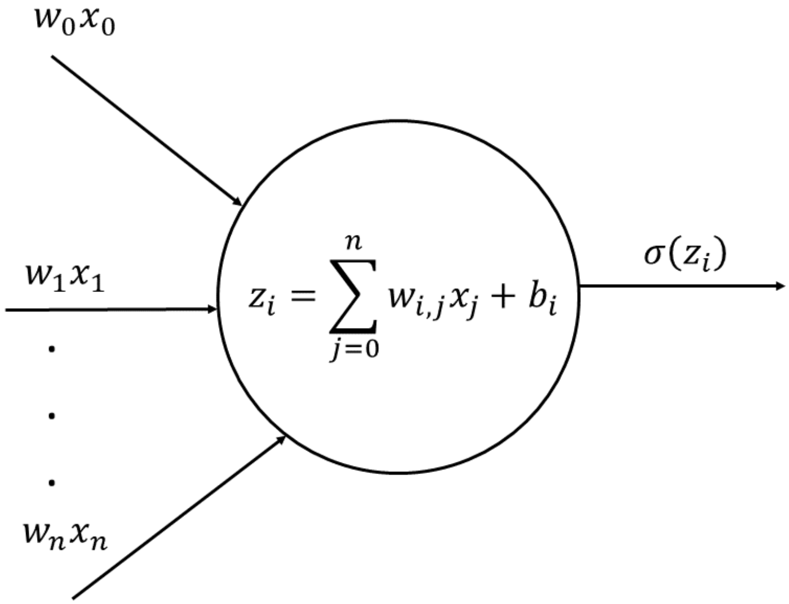

Figure 1: Schematic representation of an artificial neuron.

The selected algorithm for minimization of the loss function (eq. (23)) is the bayesian regularization, which updates the weights and biases values according to the Levenberg-Marquardt optimization (Marquardt, 1963). Backpropagation is used to calculate the Jacobian of the performance with respect to the weight and bias variables (Dan Foresee and Hagan, 1997; MacKay, 1992). The used DNN was developed using MATLAB. It is conformed by one layer which receives the input data (input layer), three intermediate layers (hidden layers) with 20 neurons each and an output layer with a single neuron which returns the simulated target values (Fig. 2).

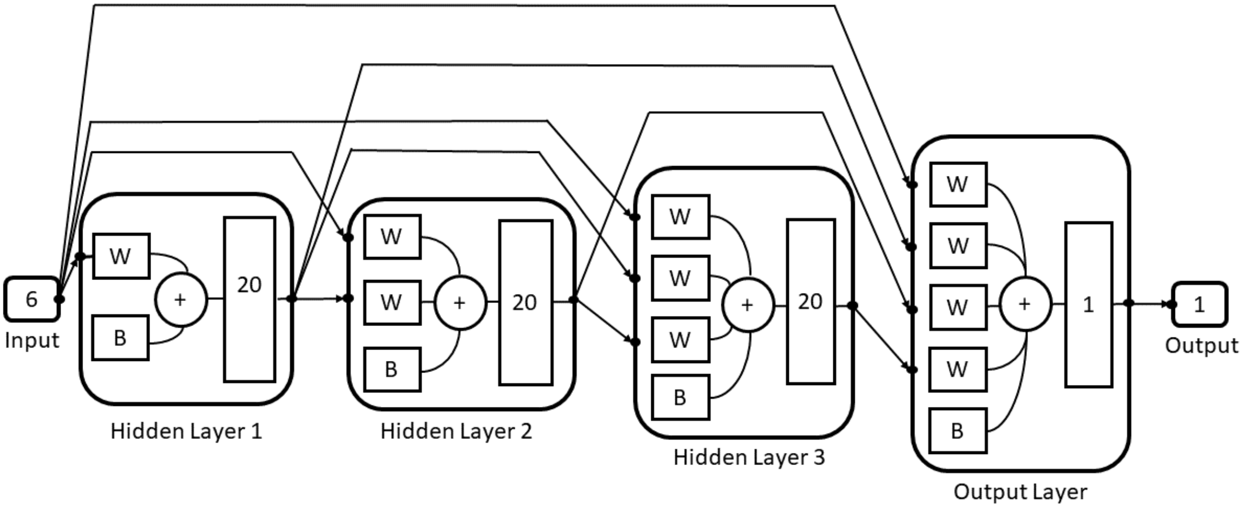

Figure 2: Schematic representation of the architecture of the trained neural network used to calculate the total moment tendencies. The neural network receives six inputs and then processes them by means of three hidden layers of 20 neurons each, and an output layer with a single neuron and one output value.

3.2 Generation of the training and validation data sets

The training procedure consists of feeding the DNN with six input values corresponding to the distribution parameters of each distribution and the total moment tendency for the *p*-th order obtained from eq. (13) as a target. The NN training algorithm then processes those values in order to establish the relationships between the data provided. This process is repeated until all input and target data is processed. The resulting trained DNN should be able to estimate the total moment tendencies from a given set of distribution parameters that falls within the ranges of the training variables. A schematic representation of the trained NN with the inputs and output is shown in Fig. 3.

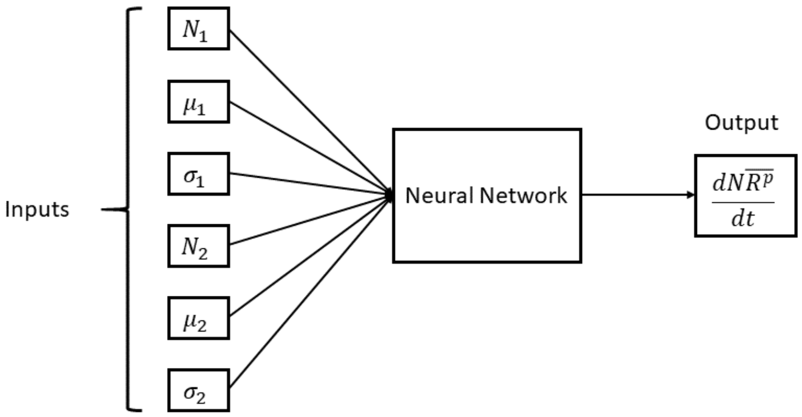

Figure 3: Neural network parameterization inputs and output. The input data are the six distribution parameters (N_1, μ_1 , σ_1, N_2, μ_2 and σ_2) needed to feed eq. (13), while the output is the p-th order total moment tendency $\left(\frac{dN\overline{R^p}}{dt}\right)$.

In order to generate the training and test data sets, 100000 drop spectra derived from the input variables are employed, over a wide range of distribution parameters (N_1, μ_1 , σ_1, N_2, μ_2 and σ_2) . Those input parameters are used to calculate the total moment rates from eq. (13) and train the DNN. Five DNNs are trained, one for each total moment tendency involved in the formulation of the parameterization (moment orders ranged from 0 to 5), with exception of the total moment of order 3, as total mass is not affected by the collision-coalescence process. The same training input parameters are used to train all NNs, varying only the target values corresponding to the total moment tendencies of each order.

The physical variables related to the input parameters are shown in Fig. 4 for a better representation of the generated training clouds. The training and test data is created using an uniformly distributed random number generator, with means and standard deviations shown in Table 1, as well as the ranges (minimum and maximum values) of each predictor variable.

Table 1: Statistical description of the input values used in the training and test data sets. The means, standard deviation and ranges are shown for each input variable.

Input Variable	Mean	Standard Deviation	Range [min, max]
Concentration (N)	250.80	144.13	[1.00; 500.00]
μ Parameter	-7.00	0.58	[-8.00; -6.00]
σ Parameter	0.20	0.06	[0.10; 0.30]

Figure 4 shows that within the ranges of the training data (concentration from 1 cm^{-3} to 500 cm^{-3}), the corresponding liquid water contents (LWC) are between 10^{-10} g cm^{-3} and 10^{-4} g cm^{-3}, with the majority of the data concentrated between the limits of 10^{-8} g cm^{-3} and 10^{-5} g cm^{-3}. Those values cover a sufficiently wide range of liquid water content to adequately represent warm clouds within the parameterization.

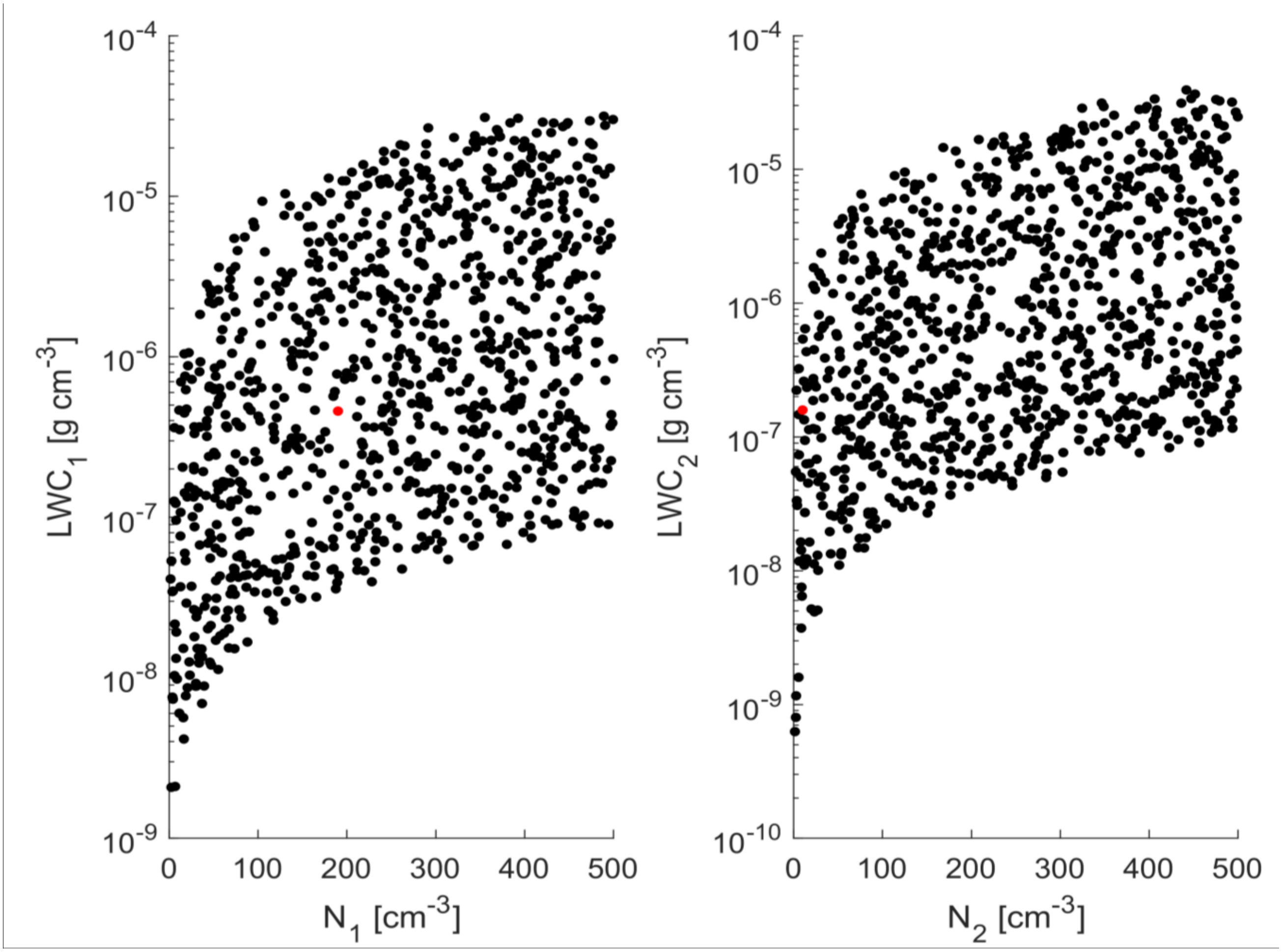

Figure 4: Scatterplot of liquid water content (LWC) calculated from the input parameters of f_1 (left) and f_2 (right) vs drop number concentration. The LWC values are obtained from the statistical moment of order 3 using the parameters depicted in Table 1, and were calculated from eq. (4). The red dots represent the initial conditions for the experiment case included in Table 4. Only every 100th data point is shown.

3.3 Training and testing of the Deep Neural Network

From the available data, 80 % is employed in training the DNN, and the remaining 20 % is used for testing purposes. The total moment tendencies (eq. 13) are solved using a trapezoidal rule, over a logarithmic radius grid between the ranges of $1\ \mu m \leq r \leq 10^4\ \mu m$. The solutions of eq. (13) are called the target values. The mean and standard deviation for each calculated total moment rate are shown in Table 2.

Table 2: Means and standard deviations of total moment tendencies (target values) for each statistical moment used. The data is calculated from eq. (13) with the distribution parameters (N_1, μ_1, σ_1, N_2, μ_2 and σ_2) as input values.

Total Moment Order	Mean	Standard Deviation
M0	-0.0021	0.0014
M1	-0.0015	0.0011
M2	-0.0009	0.0006
M4	0.0011	0.0007
M5	0.0024	0.0016

Both input and target values are normalized as follows

$$x_{norm} = \frac{x - \bar{x}}{\sigma} \qquad (24)$$

The input and target values require normalization to facilitate the work of the optimization algorithm. All nodes in each layer of the DNN use the MSE as a loss function. The training procedure for a NN consists of processing a fragment of the total training data through the network learning architecture, then determining the prognostic error and the gradient of the loss function (MSE) back through the network in order to update the weight values. This algorithm is repeated via an iterative process over all training data until the performance index (MSE) is small enough or a predefined number of passes through all data are completed. One pass through all training data is known as an epoch. In this case, a maximum number of 1000 epochs is established, and a minimum value of 10^{-7} is considered for the gradient function.

Five DNN are trained, one for each total moment tendency involved in the formulation of the parameterization (moment orders ranged from 0 to 5). A variant of the training process, known as cascade-forward neural network training, is employed. The main difference with the standard training procedure is that it includes a connection from the input and every previous layer to following layers (see Fig. 2). As with feed-forward networks, a two-or more layer cascade network can learn any finite input-target relationship arbitrarily well, given enough hidden neurons. The total moment tendencies for the statistical moment of order 3 is not calculated because the collision-coalescence process does not affect total mass.

Performance (MSE) training records for the total moment tendencies calculated from eq. (13) are depicted in Fig. 5. The speed of convergence is similar in all cases, and all networks converged at epoch 1000. This occurs because the gradient value never was below the minimum, so the training process kept refining the results until it reached the maximum number of epochs previously defined. Despite that, a good performance is achieved, with the MSE in the order of 10^{-4} for all orders of the total moment tendencies as shown in Table 3, where the best (final) MSE values for each trained DNN are manifested in detail. Since the values of the total moments are normalized in the DNN model (scale of 10^0), these values of MSE are considered as the indications of high accuracies for the scale of the problem.

Table 3: Best performance in the training process of the DNNs. The performance measures are the Mean Squared Error (MSE) and the Pearson Correlation Index. The shown data corresponds to the total moment tendencies obtained from the trained neural networks, with input values and reference targets taken from the validation data set.

Total Moment Order	Best Performance (MSE)	Correlation Index
M0	2.59e-04	0.9998
M1	3.49e-04	0.9998
M2	2.68e-04	0.9999
M4	1.80e-04	0.9999
M5	2.05e-04	0.9998

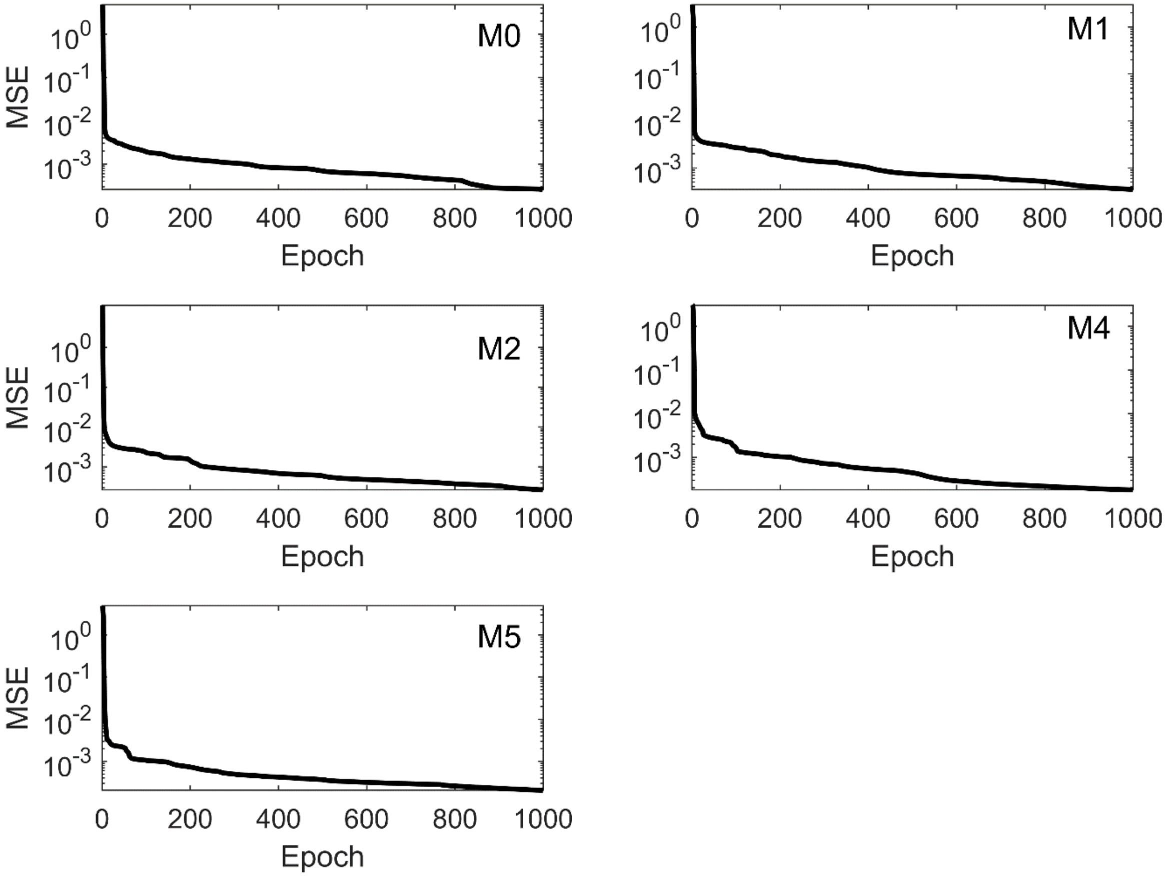

Figure 5: Performance training records of total moment tendencies for the moments from order 0 to 5. The shown data corresponds to the total moment tendencies obtained from the trained neural networks, with input values and reference targets taken from the validation data set. The performance measure is the Mean Square Error (MSE).

Regression plots for the trained networks are depicted in Fig. 6. It is a comparison between the outputs obtained from evaluating the trained neural networks using the test inputs and the targets from the test data set corresponding to each of the total moment tendencies obtained from eq. (13). Minor differences can be appreciated from the graphics, with the trained DNN models overestimating or underestimating the actual values. However, a good agreement was reached for all trained DNN, with the predicted values from the DNN matching the actual output from the solution of eq. (13) with a coefficient of correlation between 0.9998 and 0.9999 in all cases (as shown in Table 3). The axis ranges of the graphics vary because the plotted data is non-normalized, thus, there are different ranges for each of the calculated total moment tendencies.

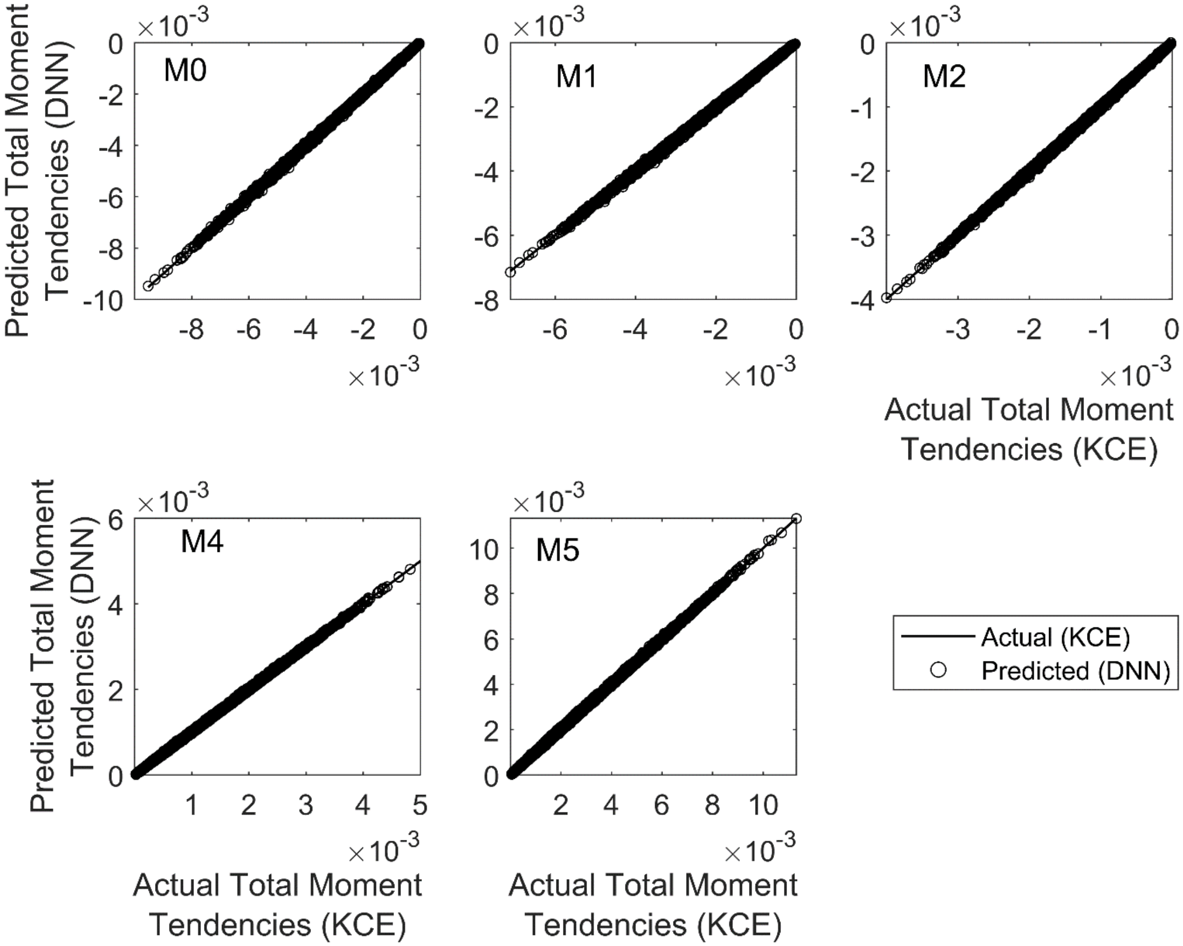

Figure 6: Regression plots for the five DNN trained. It is a comparison between the outputs obtained from evaluating the trained neural networks using the test inputs and the targets from the validation data set corresponding to each of the total moment tendencies obtained from eq. (13). The order of the statistical moments range from 0 to 5. The y axis varies for each subplot because the plotted data is non-normalized.

Experiments with non-normalized training data were performed, yielding results with MSE at least an order of magnitude higher. Those results are not shown in the present article due to the lower accuracy of the regression outputs.

Neural networks give us a better way to estimate the values of the integral (13). If the parameterization was implemented from real time calculations of the integral (13) by the trapezoidal rule every time it was necessary, it would be extremely slow. The neural networks of course do not replace the computation of integrals, but since they have the ability to learn and model complex non-linear functions, they allow (once trained) to estimate them efficiently for values of the parameters (N_1, μ_1 , σ_1, N_2, μ_2 and σ_2), for which it has not been previously calculated.

Before the widespread adoption of machine learning, the alternative previously used by other authors (Clark, 1976; Clark and Hall, 1983; Feingold et al., 1998) were the lookup tables, that are tables that stores a list of predefined values (the moment tendencies in this case). Then, in the context of our work, the lookup table is a mapping function that relates the parameters of the basis functions (N_1, μ_1 , σ_1, N_2, μ_2 and σ_2), with the total moment tendencies $\left(\frac{dN\overline{R^p}}{dt}\right)$.

However, usually, functions computed from lookup tables have a limited domain. For larger problems, the memory and the time required to access the data increase substantially. Furthermore, preferably, we need functions whose domain is a set with contiguous values. Additionally, every time we need to calculate the integral (13), a search algorithm must be executed in order to retrieve the moment tendency for a given set of parameters, and some kind of interpolation will be needed to compute moment tendencies for values of the parameters for which it has not been calculated.

The advantage of the neural networks is that all the computational effort is dedicated to the training phase. Once we trained the networks, they replace the lookup tables and are able to map efficiently the parameters of the basis functions with total moment tendencies. A significant speed up is expected since we just need to evaluate the input parameters, and there is no need to execute a searching algorithm in order to retrieve the desired information.

The codes for generating the training and validation data sets, and training of the neural networks themselves can be found at (Rodríguez-Genó and Alfonso, 2021c).4 WDM6 parameterization and experiment design

An experiment is performed with the objective of illustrating the behaviour of the ML-based parameterized model (P-DNN) and how it compares with the results of a traditional bulk parameterization and the reference model (KCE). This experiment should not be interpreted as an evaluation of the overall behaviour of P-DNN, but as an example of how it predicts the DSD and bulk variables. A detailed evaluation of the novel components of the P-DNN scheme was already carried out in the previous chapter.

4.1 Initial conditions and experiment design

The simulation lasted for $t = 900\ s$ (15 minutes) is considered for all models, with a time step of $\Delta t = 0.1\ s$. The initial parameters for the distribution functions of the parameterized model are as shown in Table 4.

Table 4: Initial parameters for the distribution functions of P-DNN. Each distribution is characterized by a concentration parameter (*N*), expected value (μ) and standard deviation (σ). The initial parameters are shown for the two lognormal distribution functions employed in the formulation of P-DNN.

Parameter	f_1	f_2
N	190 cm^{-3}	10 cm^{-3}
μ	-7.1505	-6.5219
σ	0.1980	0.1980

The values from Table 4 are well within the parameters established on Table 1, and were set following (Clark, 1976). They were chosen, as they are a good representation of the training data on which the neural networks were trained. The initial spectrum for the KCE was calculated from these parameters to ensure the same initial conditions for both models. A 300-point logarithmic equidistant grid was generated for the integration of the KCE, with radii values in the range of $0.25\ \mu m \leq r \leq 2.6 \times 10^4\ \mu m$. Equations (17) and (18) were used to transform the output of both models to make them comparable, while the bulk quantities from the KCE were integrated from the calculated spectra.

4.2 WDM6 parameterization

To better establish the accuracy of the P-DNN, an extra parameterization was included in the comparison with the reference solution. The selected parameterization is the WRF Double Moment 6-class bulk mode (WDM6) (Lim and Hong, 2010), which was chosen for being commonly used and being implemented in a well-known three-dimensional atmospheric model (WRF). The collision-coalescence section of that parameterization is explained in detail in (Cohard and Pinty, 2000), and treats the main warm microphysical processes in the context of a two-moment framework. A scheme of such a type is believed to be a pragmatic compromise between over-simplified bulk parametrizations of precipitations as proposed by (Kessler, 1969) and very detailed bin models that are computationally too cumbersome for practical use in 3D mesoscale models. Inclusion of a prognostic equation for the number concentration of raindrops provides a better insight into the growth of large drops, which in turn can only improve the time evolution of the mixing ratios.

The scheme makes use of analytical solutions of some microphysical processes, after reasonable simplifications. This has been done with an elaborate function, the generalized gamma distribution that enables fine tuning of droplet/drop spectral shape through the adjustment of two free-dispersion parameters. All the tendencies, except the autoconversion of the cloud droplets, are parametrized on the basis of continuous integrals that encompass the whole range of drop diameters. With this method, the treatment of autoconversion is the weakest link in the scheme because this process acts in the diameter range where the fuzzy transition between cloud droplets and raindrops is hardly compliant with a bimodal and spectrally wide (from zero to infinity) representation of the drops. This model is represented in the following sections as P-CP2000. For comparison purposes, all simulations share the same initial conditions. It should be noted that WDM6, being a conventional two-moment scheme, is focused on the evolution of the moments of order zero and three of a truncated gamma distribution function. The code for the WDM6 parameterization and related files can be found at (Rodríguez-Genó and Alfonso, 2021d)**.**

5 Discussion of results

The results shown in this section were obtained using the parameterized model COLNETv1.0.0. The source code can be found at (Rodríguez-Genó and Alfonso, 2021a), while the scripts for reproducing the figures are archived at (Rodríguez-Genó and Alfonso, 2021b)

5.1 Spectra comparison

The output of this parameterized Deep Neural Network model (P-DNN) are the updated distribution parameters at every time step (N_1, μ_1 , σ_1, N_2, μ_2 and σ_2). The physical variables related to the moments of the distributions, such as mean radius or liquid water content (LWC) are diagnosed from those parameters. Besides, we can calculate the shape and scale of the drop spectrum at any given time, by integrating the distribution functions defined by its parameters.

Figure 7 shows a comparison between the mass density spectra derived from P-DNN and KCE models for three chosen times (300 s, 600 s and 900 s).

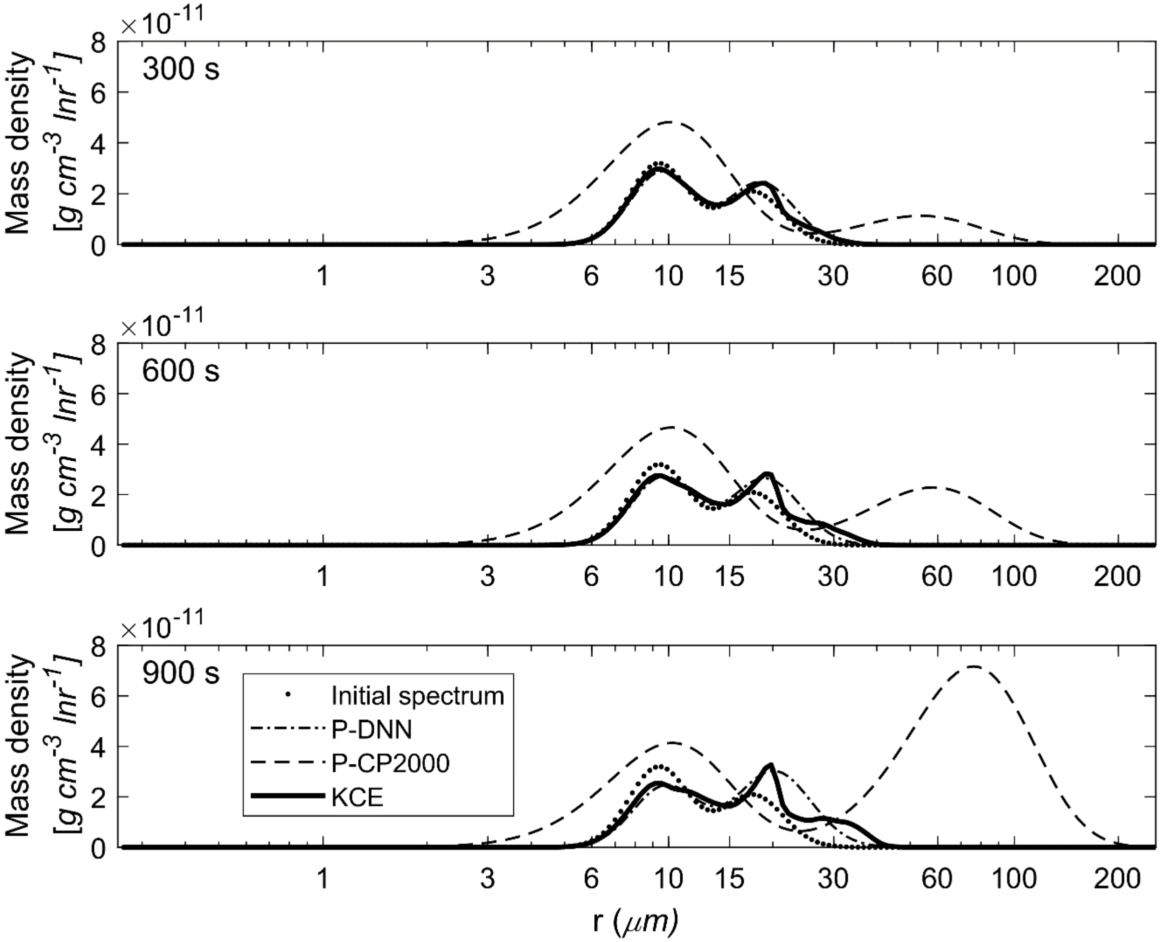

Figure 7: Mass density functions from P-DNN, P-CP2000 and KCE. The represented times are 300 s, 600 s and 900 s, from top to bottom. Equation (17) was used to transform the drop number concentration spectra from P-DNN to the mass density spectra.

At 300 s (first row of Fig. 7), there is a slow development of the total spectrum, with a clear mass transfer between both modes of the presented models. The parameter-generated spectrum from P-DNN fits well the reference solution, with a slight overestimation of the maximum mass in the second mode. The mean radius of the distributions are well represented by P-DNN. At 600 s and 900 s (second and third row of Fig. 7), there is a development of a third mode in the evolution of KCE, that is not reproduced by P-DNN, producing instead a wider second mode, representing well the mean radius and mass distribution. The first mode is accurately represented at those times. An increase in mean radius can be observed, due to the effect of the collision-coalescence process.

The simulation results with P-CP2000 are clearly different from the others. The first noticeable difference is the existence of droplets that are smaller than the initial distribution. This is caused by the fixed distribution parameters employed in its formulation. The slope parameter is determined by an analytical expression and evolves with time within certain limits, but the parameters related to the spectral breadth are held fixed. For more information please refer to (Cohard and Pinty, 2000). Besides that,, P-CP2000 performs poorly at all the represented simulation times, when compared with KCE. It presents pronounced tendency to go ahead of the KCE, leading to a faster-than-normal development of larger drops. Particularly, the mass transfer is very noticeable at the end of the simulation. However, the first mode of P-CP2000 does not decrease proportionally, which leads to think that there are a lot of small drops and a few big drops accounting for that increase in mass by the end of the simulation.

Figure 8 shows a comparison between the drop number concentration spectra derived from P-DNN, P-CP2000 and KCE for three chosen times (300 s, 600 s and 900 s). A generally good agreement is appreciated at all times for P-DNN, with its spectra slightly underestimating the results from KCE. As the collision-coalescence process decreases the drop number concentration, there is no noticeable increase in the number of drops in the second mode of the distributions. However, an increase in the mean radius is observed, that is consistent with the behaviour described in Fig. 7, where a related mass transfer between both distribution functions is seen.

Regarding P-CP2000, its spectra underestimate the KCE, and the lack of a second mode reaffirms the behaviour shown in Fig. 7. However, being a conventional bulk parameterization, its strong points are not related to the description of the drop spectra, but to the representation of bulk quantities such as the total number concentration and mass content of the clouds.

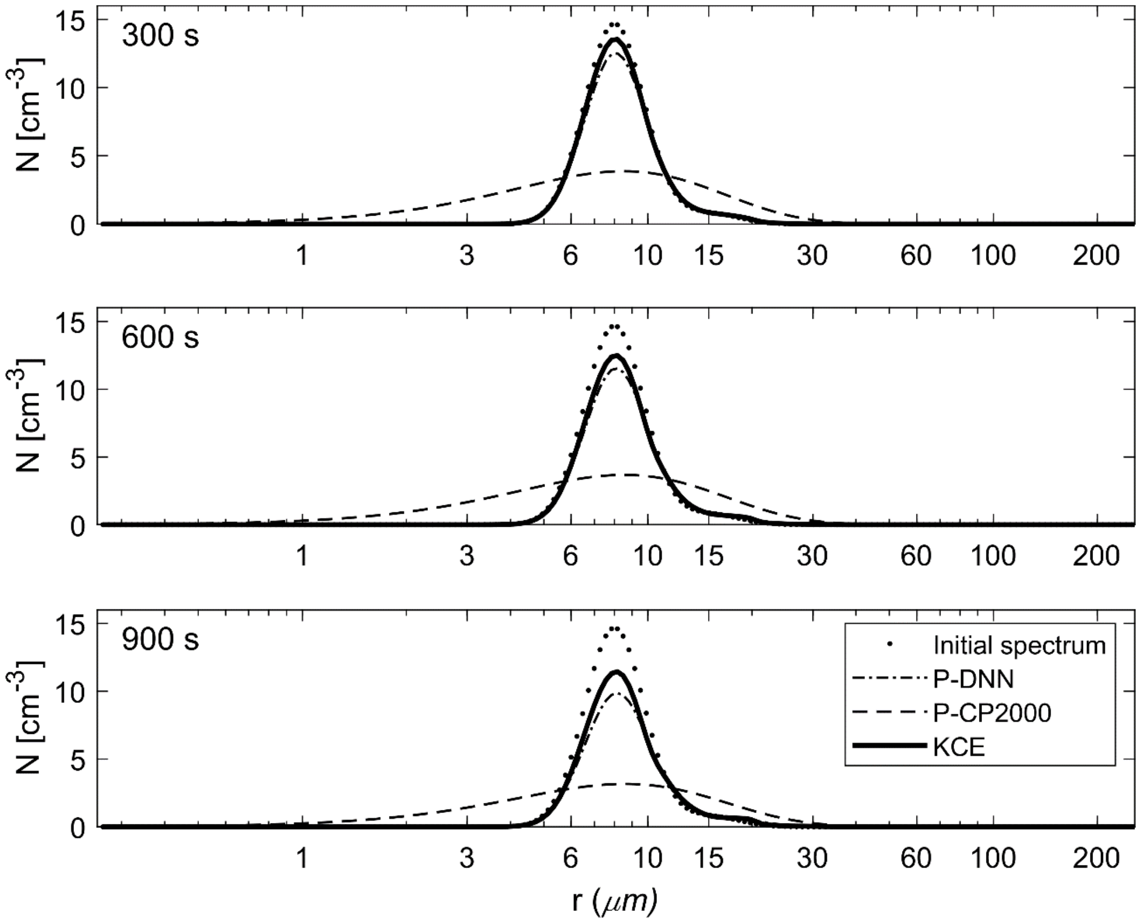

Figure 8: Drop number concentration spectra P-DNN, P-CP2000 and KCE. The selected times are 300 s, 600 s and 900 s, from top to bottom. Equation (18) was used to transform the mass density spectra from KCE to the drop number concentration spectra.

5.2 Bulk quantities comparison

Figure 9 shows a comparison of two main bulk quantities (total number concentration and mean radius) obtained from P-DNN, P-CP2000 and KCE. The concentration and mean radius of KCE were obtained by integrating the drop number concentration spectra for the corresponding moment order (0 and 1 respectively). As expected, number concentration decreases with time, due to the coalescence of drops, ranging from an initial value of 200 cm^{-3} to around 160 cm^{-3} in KCE. The predicted concentration from P-DNN underestimates the KCE values in most of the simulation, with the differences reaching 10 cm^{-3} at 900 s. A relatively better representation of drop number concentration is achieved by the P-CP2000 model, showing values closer to KCE, although it reaches the same differences as P-DNN by the end of the simulation.

A similar behaviour is observed in the mean radius results, with a growth in the drop size consistent with the decreasing values on the drop number concentration for P-DNN, but differences are small with the highest error of 5 μm. However, the results fit well enough the reference solution to consider including this microphysical parameterization in a weather model. This consistent behaviour of the mean radius and number concentration values points to a conservation of mass, a compulsory condition in the collision-coalescence process. However, P-CP2000 performs somehow worse than P-DNN for the mean radius, with the mean difference almost reaching 10 μm, although it shows a similar monotony to both the KCE and P-DNN models.

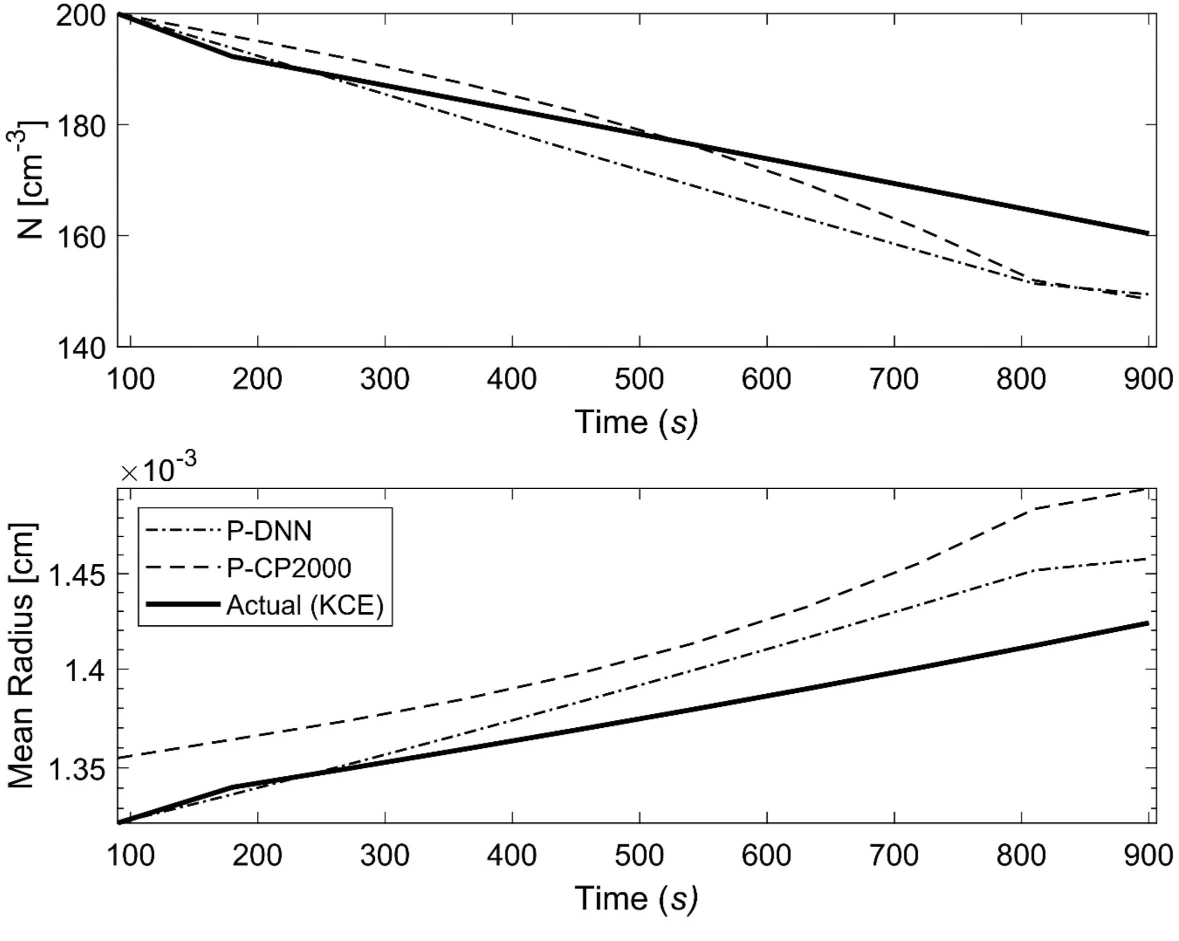

Figure 9: Drop number concentration (top) and mean radius (bottom) comparison with KCE. The concentration and mean radius of KCE were obtained by integrating the drop number concentration spectra for the corresponding moment order (0 and 1 respectively). The data points are plotted every 60 s.

Figure 10 depicts the evolution of two main bulk quantities (drop number concentration and liquid water content) for the individual distributions that conform P-DNN (f_1 and f_2), as well as the combined (total) values of the variables (calculated as

$f_1 + f_2$). Regarding concentration, a decrease in f_1 values is observed, due to the coalescence process, while a consistent increase in f_2 is also appreciated. The increase in the concentration of f_2 is not as marked due to the collision-coalescence process as well. However, a general decrease of the total concentration value represents well the theory and observations of the parameterized process.

The liquid water content (LWC) values (diagnosed) are depicted only to verify that mass is conserved under the formulation of P-DNN. The LWC of each of the distribution functions (f_1 and f_2) were obtained from the corresponding moment (order 3) calculated from eq. (4). Effectively, the mass content retains a value of $6.1739 \times 10^{-7}\ g\ cm^{-3}$ during the entire simulation, with a proportional mass transfer between f_1 and f_2.

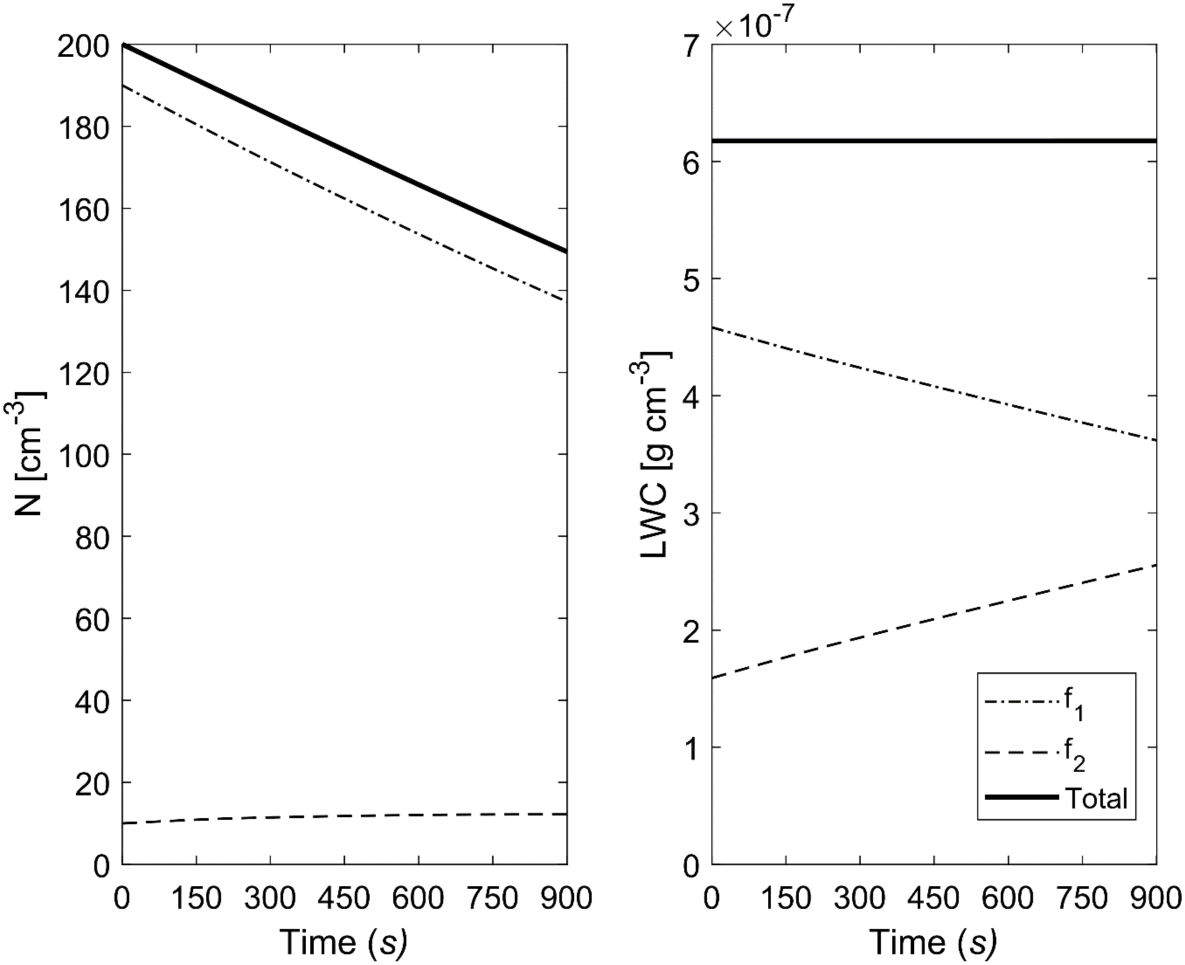

Figure 10: Evolution of drop number concentration N (left) and liquid water content LWC (right) of the individual distributions that conform P-DNN. The liquid water content of each of the distribution functions (f_1 and f_2) were obtained from the corresponding moment (order 3) calculated from eq. (4). The combined (total) values of the variables are also shown and were calculated from eq. (5).

5.3 Total moment errors

An analysis of the predicted total moments was performed with the objective to further test the precision of P-DNN, due to the importance of the statistical moments in calculating physical variables such as mean radius and LWC. Table 5 shows the mean percent errors of the total moments predicted by P-DNN and P-CP2000. The percent error is taken relative to the moments of KCE. The data was obtained by calculating the mean of the percent errors of the entire simulation. The moments of KCE were calculated by integrating the reference drop number concentration spectra using eq. (3), while the total moments from P-DNN and P-CP2000 were calculated using the predicted distribution parameters and solving eq. (5). The defined gamma distribution equations for the moments, are used in the case of P-CP2000. A reasonable degree of accuracy was achieved by P-DNN, with the mean error never surpassing the 4 %. However, the data shows that the total moments of order 0 to 2 are usually underestimated, while those of order 4 and 5 are slightly overestimated. This could result in the calculations of drop number concentration values lower than the actual ones, as seen in Fig. 9. As for P-CP2000, the model is not formulated to predict individual moments other than the zeroth and third moments. Thus, it performs badly in representing the other moments of the distributions, as observed in the mean percent error, which reaches almost -61% for the moment of order five. That value is a great difference from the zeroth moment for example, whose percent error is only -1.3 %. This result indicates that the modelling philosophy of P-DNN is adequate to represent the evolution of individual moments within certain ranges, when compared with more conventional bulk schemes.

Table 5: Total moment mean errors. The percent error is taken relative to the moments of KCE. The shown data was obtained by calculating the mean of the percent errors of the entire simulation.

Total Moment Order	Mean Percent Error P-DNN	Mean Percent Error P-CP2000
M0	-3.3479	-1.2718
M1	-2.6437	27.0500
M2	-1.4969	27.0370
M4	1.1249	9.2037
M5	0.7205	-60.8886

Figure 11 shows the time evolution of the percent error of the total moments throughout the simulation for P-DNN. The percent error is taken relative to the moments of KCE. The moments of KCE were calculated by integrating the reference drop number concentration spectra using eq. (3), while the total moments from P-DNN were calculated using the predicted distribution parameters to solve eq. (5). The error of total moment of order 3 is zero during the entire simulation because mass is not affected by the collision-coalescence process. The total moments from order 0, 1 and 2 overestimate the KCE in the first 300 s of simulation, underestimating them for the rest of the P-DNN run, with the percent error reaching a minimum value of -8 %. The opposite behaviour is appreciated for the total moments of order 4 and 5, where they initially underestimate the KCE, overestimating it for the rest of the simulation. However, for these orders the percent error is usually lower, with a maximum of 4 %. Generally, P-DNN is performing well, with the percent error never reaching the 10 % threshold. However, further analysis on this topic is recommended, to improve the accuracy of the parameterization.

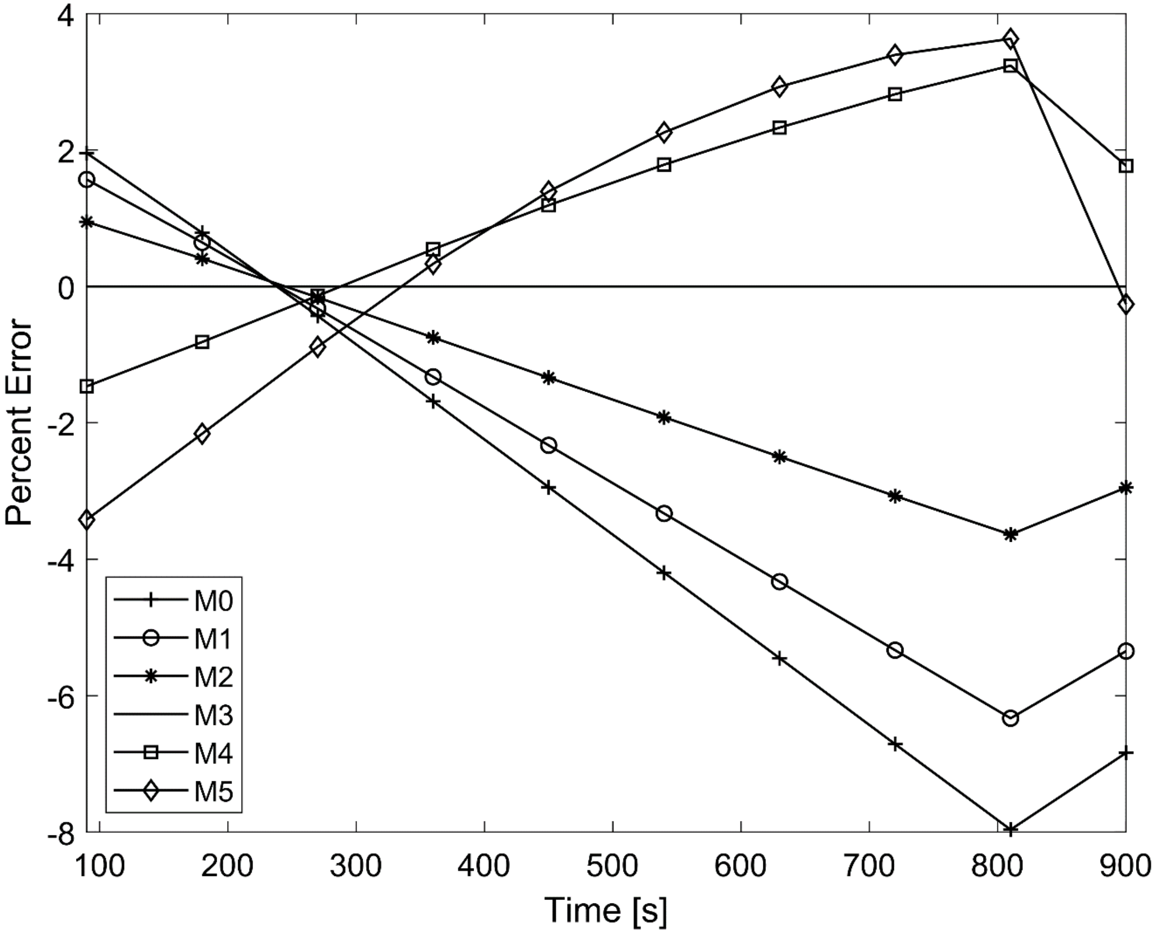

475 **Figure11: Time evolution of the errors corresponding to the predicted moments from P-DNN. The percent error is taken relative to the moments of KCE. The moments of KCE were calculated by integrating the reference drop number concentration spectra using eq. (3), while the total moments from the P-DNN were calculated using the predicted distribution parameters to solve eq. (5).**

6 Conclusions

480 A hybrid parameterization for the process of collision-coalescence based on the methodology of basis functions employing a linear combination of two lognormal distributions was developed and implemented.All the parameters of the distributions are derived from the total moment tendencies and calculated by means of five trained deep neural networks. By doing this, we obtained a parameterized model that determines the distribution parameters' evolution, hence, the evolution of the DSD. The

physical variables are diagnosed from the distribution moments. Within the framework of this parameterized model, there is no artificial separation of the DSD. Instead, we consider a full set of distribution parameters for each of the distribution functions that are considered in the formulation of the parameterization, in order to describe the DSD in radius space. This kind of microphysical parameterization allows the use of an arbitrary number of statistical density functions in linear combination to reproduce the drop spectrum.

The novel components of the P-DNN model were evaluated in Chapter 3, demonstrating the precision and ability of the ML method to reproduce the rates of the total moments due to collision-coalescence. One experiment was performed to illustrate the behaviour of the proposed ML formulation at the initial stages of cloud formation. The simulation results from P-DNN showed good agreement when compared to a reference solution (KCE) and a conventional bulk scheme (P-CP2000), for both the predicted DSD and the bulk quantities considered. According to the comparison with the bulk model, the main strength of the DNN model is the superior ability to represent the evolution of individual moments of the distribution functions, because of its formulation based on time-varying distribution parameters. The total moment tendencies were well predicted using the trained DNNs, improving the computational performance of the original formulation. An analysis of the accuracy of the predicted total moments of P-DNN was performed, with the percent error relative to the KCE never exceeding 10 %. However, there is room for improvement in the calculations of the total moments, which is the recommendation of the authors to retrain the DNNs with a finer resolution in the parameters' values, and with a wider range of values in order to cover all possible combination of parameters. In addition, the use of ML eliminated the requirement of integrating the total moment tendencies at each time step, and the use of memory expensive lookup tables for each predicted moment is no longer needed under this formulation.

The presented way to simulate the evolution of the droplet spectra due to collision-coalescence falls within the framework developed by Clark(1976) and Clark and Hall(1983). Under this modelling philosophy, a dynamic framework has been established in Rodríguez-Genó and Alfonso(2021e). To obtain a full warm cloud model, an extension of this neural network algorithm applied to condensation is proposed, following the same methodology of series of basis functions. A parameterization scheme such as this could be included in regional weather and climate models, as its initial conditions can be calculated from variables needed by more traditional bulk models.

Author contributions

Léster Alfonso performed the conceptualization of the article, methodology, funding acquisition, resources, supervision and reviewing and editing the original draft. Camilo Fernando Rodríguez Genó realized the formal analysis, investigation, software and code development, validation, visualization, and writing the original draft preparation.

Code availability

The current version of *COLNET (COLNETv1.0.0)* used to produce the results presented in this paper is archived on Zenodo (https://doi.org/10.5281/zenodo.4740061) under the *GNU Affero General Public License v3 or later* licence, as well as all dependency scripts to run the model. The outputs of the model used to generate the figures included in the present paper are also included. The scripts used in the generation of training data sets and for training the neural networks used in *COLNETv1.0.0* can be found on Zenodo (https://doi.org/10.5281/zenodo.4740129), while the codes for plotting the figures are stored at https://doi.org/10.5281/zenodo.4740184. The original code of the explicit bin model is archived at https://www2.meteo.uni-bonn.de/forschung/gruppen/tgwww/people/abott/fortran/coad1d.f, and have been used with the permission of the author. The code used for the WDM6 parameterization simulation can be found on Zenodo (https://doi.org/10.5281/zenodo.5196706). The models and related scripts were written using MATLAB R2020a under license number 40816183, with exception of the explicit model, which is coded on FORTRAN 77.

Competing interests

The authors declare that they have no conflict of interests.

Acknowledgments

Camilo Fernando Rodríguez-Genó is a doctoral student from Programa de Posgrado en Ciencias de la Tierra at Universidad Nacional Autónoma de México, and received fellowship 587822 from Consejo Nacional de Ciencia y Tecnología (CONACyT). This study was funded by grant no. CB-284482 from the Consejo Nacional de Ciencia y Tecnología (SEP-CONACyT).

Financial support

This research has been supported by the Consejo Nacional de Ciencia y Tecnología (CONACyT) by means of grant no. CB-284482 and fellowship no. 587822.

References

Alfonso, L. and Zamora, J. M.: A two-moment machine learning parameterization of the autoconversion process, Atmos. Res., 249, 105269, doi:10.1016/j.atmosres.2020.105269, 2021.

Alfonso, L., Raga, G. B. and Baumgardner, D.: The validity of the kinetic collection equation revisited, Atmos. Chem. Phys., 8(4), 969–982, doi:10.5194/acp-8-969-2008, 2008.

Alfonso, L., Raga, G. B. and Baumgardner, D.: A Monte Carlo framework to simulate multicomponent droplet growth by stochastic coalescence, in Applications of Monte Carlo method in science and engineering, edited by S. Mordechai, InTech., 2011.

Berry, E. X.: Cloud droplet growth by collection, j. atmos. Sci., 24(6), 688–701, doi:10.1175/1520-0469(1967)024<0688:CDGBC>2.0.CO;2, 1967.

Berry, E. X. and Reinhardt, R. L.: An analysis of cloud drop growth by collection: Part I. Double distributions, J. Atmos. Sci., 31(7), 1814–1824, doi:10.1175/1520-0469(1974)031<1814:AAOCDG>2.0.CO;2, 1974.

Bott, A.: A flux method for the numerical solution of the stochastic collection equation, J. Atmos. Sci., 55(13), 2284–2293, doi:10.1175/1520-0469(1998)055<2284:AFMFTN>2.0.CO;2, 1998a.

Bott, A.: Program for the solution of the stochastic coalescence equation: One-dimensional cloud microphysics., 1998b.

Brenowitz, N. D. and Bretherton, C. S.: Prognostic validation of a neural network unified physics parameterization, Geophys. Res. Lett., 45(12), 6289–6298, doi:10.1029/2018GL078510, 2018.

Clark, T. L.: Use of log-normal distributions for numerical calculations of condensation and collection, J. Atmos. Sci., 33(5), 810–821, doi:10.1175/1520-0469(1976)033<0810:UOLNDF>2.0.CO;2, 1976.

Clark, T. L. and Hall, W. D.: A cloud physical parameterization method using movable basis functions: Stochastic coalescence parcel calculations, J. Atmos. Sci., 40(7), 1709–1728, doi:10.1175/1520-0469(1983)040<1709:ACPPMU>2.0.CO;2, 1983.

Cohard, J.-M. and Pinty, J.-P.: A comprehensive two-moment warm microphysical bulk scheme. I: Description and tests, Q. J. R. Meteorol. Soc., 126(566), 1815–1842, doi:10.1256/smsqj.56613, 2000.

Dan Foresee, F. and Hagan, M. T.: Gauss-Newton approximation to Bayesian learning, in Proceedings of International Conference on Neural Networks (ICNN'97), vol. 3, pp. 1930–1935, IEEE, Houston., 1997.

Feingold, G. and Levin, Z.: The lognormal fit to raindrop spectra from frontal convective clouds in Israel, J. Clim. Appl. Meteorol., 25(10), 1346–1363, doi:10.1175/1520-0450(1986)025<1346:TLFTRS>2.0.CO;2, 1986.

Feingold, G., Walko, R. L., Stevens, B. and Cotton, W. R.: Simulations of marine stratocumulus using a new microphysical parameterization scheme, Atmos. Res., 47–48, 505–528, doi:10.1016/S0169-8095(98)00058-1, 1998.

Gillespie, D. T.: The stochastic coalescence model for cloud droplet growth, J. Atmos. Sci., 29(8), 1496–1510, doi:10.1175/1520-0469(1972)029<1496:TSCMFC>2.0.CO;2, 1972.

Hall, W. D.: A detailed microphysical model within a two-dimensional dynamic framework: Model description and preliminary results, J. Atmos. Sci., 37(11), 2486–2507, doi:10.1175/1520-0469(1980)037<2486:ADMMWA>2.0.CO;2, 1980.

Huang, W. T. K.: Reformulation of the Milbrandt and Yau microphysics parameterization: A triple-moment lognormal scheme, McGill University. [online] Available from: https://www.proquest.com/dissertations-theses/reformulation-milbrandt-yau-microphysics/docview/2512357588/se-2?accountid=12874, 2014.

Kessler, E.: On the distribution and continuity of water substance in atmospheric circulations, in Meteorological Monographs, vol. 10, pp. 1–84, American Meteorological Society, Boston, MA., 1969.

Khain, A., Pokrovsky, A., Pinsky, M., Seifert, A. and Phillips, V.: Simulation of Effects of Atmospheric Aerosols on Deep Turbulent Convective Clouds Using a Spectral Microphysics Mixed-Phase Cumulus Cloud Model. Part I: Model Description and Possible Applications, J. Atmos. Sci., 61(24), 2963–2982, doi:10.1175/JAS-3350.1, 2004.

Khain, A., Lynn, B. and Dudhia, J.: Aerosol effects on intensity of landfalling hurricanes as seen from simulations with the wrf model with spectral bin microphysics, J. Atmos. Sci., 67(2), 365–384, doi:10.1175/2009JAS3210.1, 2010.

Khain, A. P., Beheng, K. D., Heymsfield, A., Korolev, A., Krichak, S. O., Levin, Z., Pinsky, M., Phillips, V., Prabhakaran, T., Teller, A., van den Heever, S. C. and Yano, J.-I.: Representation of microphysical processes in cloud-resolving models: Spectral (bin) microphysics versus bulk parameterization, Rev. Geophys., 53(2), 247–322, doi:10.1002/2014RG000468, 2015.

Khairoutdinov, M. and Kogan, Y.: A new cloud physics parameterization in a large-eddy simulation model of marine stratocumulus, Mon. Weather Rev., 128(1), 229–243, doi:10.1175/1520-0493(2000)128<0229:ANCPPI>2.0.CO;2, 2000.

Koza, J. R., Bennett, F. H., Andre, D. and Keane, M. A.: Automated design of both the topology and sizing of analog electrical circuits using genetic programming, in Artificial Intelligence in Design ’96, edited by J. S. Gero and F. Sudweeks, pp. 151–170, Springer Netherlands, Dordrecht., 1996.

Lee, K. W., Chen, J. and Gieseke, J. A.: Log-normally preserving size distribution for brownian coagulation in the free-molecule regime, Aerosol Sci. Technol., 3(1), 53–62, doi:10.1080/02786828408958993, 1984.

Lee, K. W., Lee, Y. J. and Han, D. S.: The log-normal size distribution theory for Brownian coagulation in the low knudsen number regime, J. Colloid Interface Sci., 188(2), 486–492, doi:10.1006/jcis.1997.4773, 1997.

Lim, K.-S. S. and Hong, S.-Y.: Development of an effective double-moment cloud microphysics scheme with prognostic cloud condensation nuclei (CCN) for weather and climate models, Mon. Weather Rev., 138(5), 1587–1612, doi:10.1175/2009MWR2968.1, 2010.

Long, A. B.: Solutions to the droplet collection equation for polynomial kernels, J. Atmos. Sci., 31(4), 1040–1052, doi:10.1175/1520-0469(1974)031<1040:STTDCE>2.0.CO;2, 1974.

MacKay, D. J. C.: Bayesian interpolation, Neural Comput., 4(3), 415–447, doi:10.1162/neco.1992.4.3.415, 1992.

Marquardt, D. W.: An algorithm for least-squares estimation of nonlinear parameters, J. Soc. Ind. Appl. Math., 11(2), 431–441, doi:10.1137/0111030, 1963.

Marshall, J. S. and Palmer, W. M. K.: The distribution of raindrops with size, J. Meteorol., 5(4), 165–166, doi:10.1175/1520-0469(1948)005<0165:TDORWS>2.0.CO;2, 1948.

Milbrandt, J. A. and McTaggart-Cowan, R.: Sedimentation-induced errors in bulk microphysics schemes, J. Atmos. Sci., 67(12), 3931–3948, doi:10.1175/2010JAS3541.1, 2010.

Milbrandt, J. A. and Yau, M. K.: A multimoment bulk microphysics parameterization. Part I: Analysis of the role of the spectral shape parameter, J. Atmos. Sci., 62(9), 3051–3064, doi:10.1175/JAS3534.1, 2005.

Mitchell, T.: Machine Learning, McGraw Hill, New York., 1997.

Morrison, H., Thompson, G. and Tatarskii, V.: Impact of cloud microphysics on the development of trailing stratiform precipitation in a simulated squall line: Comparison of one- and two-moment schemes, Mon. Weather Rev., 137(3), 991–1007, doi:10.1175/2008MWR2556.1, 2009.

Noh, Y., Oh, D., Hoffmann, F. and Raasch, S.: A cloud microphysics parameterization for shallow cumulus clouds based on lagrangian cloud model simulations, J. Atmos. Sci., 75(11), 4031–4047, doi:10.1175/JAS-D-18-0080.1, 2018.

Pruppacher, H. R. and Klett, J. D.: Microphysics of clouds and precipitation, Springer Netherlands, Dordrecht., 2010.

Rasp, S., Pritchard, M. S. and Gentine, P.: Deep learning to represent subgrid processes in climate models, Proc. Natl. Acad. Sci., 115(39), 9684–9689, doi:10.1073/pnas.1810286115, 2018.

Rodríguez-Genó, C. F. and Alfonso, L.: COLNETv1.0.0, , doi:10.5281/ZENODO.4740061, 2021a.

Rodríguez-Genó, C. F. and Alfonso, L.: COLNETv1.0.0 graphics generation scripts, , doi:10.5281/ZENODO.4740184, 2021b.

Rodríguez-Genó, C. F. and Alfonso, L.: COLNETv1.0.0 neural network training scripts, , doi:10.5281/ZENODO.4740129, 2021c.

Rodríguez-Genó, C. F. and Alfonso, L.: CP2000CCv1.0.0 WDM6 Parameterization,doi:https://doi.org/10.5281/zenodo.5196706, 2021d.

Rodríguez-Genó, C. F. and Alfonso, L.: Sedimentation calculations within an Eulerian framework using series of basis functions, Q. J. R. Meteorol. Soc., 147(736), 2053–2066, doi:10.1002/qj.4009, 2021e.

Russell, S. and Norvig, P.: Artificial intelligence: a modern approach, Third Edit., Prentice Hall., 2010.

Schmidhuber, J.: Deep learning in neural networks: An overview, Neural Networks, 61, 85–117, doi:10.1016/j.neunet.2014.09.003, 2015.

Seifert, A. and Beheng, K. D.: A double-moment parameterization for simulating autoconversion, accretion and selfcollection, Atmos. Res., 59–60, 265–281, doi:10.1016/S0169-8095(01)00126-0, 2001.

Seifert, A. and Rasp, S.: Potential and limitations of machine learning for modeling warm-rain cloud microphysical processes, J. Adv. Model. Earth Syst., 12(12), doi:10.1029/2020MS002301, 2020.

von Smoluchowski, M.: Drei vorträge über diffusion, Brownsche molekularbewegung und coagulation von kolloidteilchen [Part 1], Phys. Zeitschrift, 17(22), 557–571, 1916a.

von Smoluchowski, M.: Drei vorträge über diffusion, Brownsche molekularbewegung und koagulation von kolloidteilchen [Part 2], Phys. Zeitschrift, 17(23), 585–599, 1916b.

Sobhani, N., Loft, R., Gettelman, A., Chen, C. C. and Gagne, D. J., I.: Using Machine Learning to emulate critical cloud microphysical processes, in American Geophysical Union, Fall Meeting 2018, pp. IN13C-0686., 2018.

Straka, J. M.: Cloud and precipitation microphysics, Cambridge University Press, Cambridge., 2009.

Thompson, G., Field, P. R., Rasmussen, R. M. and Hall, W. D.: Explicit forecasts of winter precipitation using an improved bulk microphysics scheme. Part II: Implementation of a new snow parameterization, Mon. Weather Rev., 136(12), 5095–5115, doi:10.1175/2008MWR2387.1, 2008.

Thompson, P. D.: A transformation of stochastic equation for droplet coalescence, Bull. Am. Meteorol. Soc., 49(5), 596, 1968.

Ulbrich, C. W.: Natural variations in the analytical form of the raindrop size distribution, J. Clim. Appl. Meteorol., 22(10), 1764–1775, doi:10.1175/1520-0450(1983)022<1764:NVITAF>2.0.CO;2, 1983.